THE JOURNAL OF PHYSICAL CHEMISTRY B

ARTICLE

pubs.acs.org/JPCB

Re-Evaluation of Rhodopsin's Relaxation Kinetics Determined from Femtosecond Stimulated Raman Lineshapes

David W. McCamant*

Department of Chemistry, University of Rochester, 120 Trustee Road, Rochester, New York 14627, United States

ABSTRACT: This work presents a theoretical treatment of the vibrational line shape generated in a femtosecond stimulated Raman spectroscopy (FSRS) experiment under conditions in which the probed vibration undergoes a significant frequency shift during its free induction decay. This theory is applied to simulate the FSRS lineshapes previously observed in rhodopsin (Kukura et al. *Science* **2005**, *310*, 1006). The previously determined relaxation times for formation of the trans-photoproduct of rhodopsin were calculated using an incorrect equation for the time dependence of the observed frequency shifts. Here the data are reanalyzed by calculation of the corrected frequency sweep occurring during the vibrational free induction decay. It is shown that the calculated frequency shifts and general conclusions of the original work are sound but that the coherent vibrational frequency shifts of the C_{10}, C_{11}, and C_{12} hydrogen-out-of-plane vibrations occur with a 140 fs time constant rather than the previously reported 325 fs time constant. This time constant provides an important constraint for models of the dynamics of the *cis* to *trans* isomerization process.

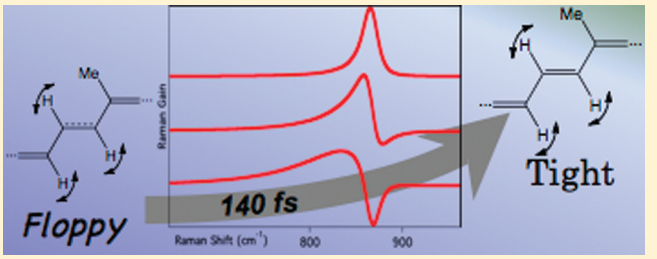

INTRODUCTION

In 2005, Kukura, McCamant, Yoon, Wandschneider, and Mathies published a ground-breaking spectroscopic study of the ultrafast dynamics of rhodopsin, the mammalian photoactive retinal pigment.[1] Their femtosecond stimulated Raman spectroscopy (FSRS) results showed that the molecular isomerization that forms the primary event in vision is completed on the ground electronic-state surface. Rhodopsin, a transmembrane protein in the G-protein coupled receptor family, is activated when its covalently bound 11-*cis* retinal absorbs light and isomerizes to all-*trans* retinal in ~200 fs (see Figure 1).[2] Previous work by Mathies and co-workers had established that the cis−trans isomerization was complete in 200 fs and that the photoproduct present by ~0.5 ps was definitely in the all-trans configuration, though highly twisted along the carbon backbone.[3−7] These conclusions were further supported by time-resolved fluorescence and transient absorption anisotropy.[8,9] Recently, Mathies, Garavelli, Cerullo, and co-workers established that the retinal distorts to reach the conical intersection between the excited and ground electronic states in 80 fs, following the absorption of light, and that the photoproduct absorption spectrum appears abruptly at 150 fs.[10]

In reference 1, Kukura et al. (including this author) probed rhodopsin's photochemical dynamics using FSRS, a vibrational spectroscopy with simultaneous 90 fs time resolution and better than 15 cm^{-1} spectral resolution.[10−12] In that work, we were able to observe the time-dependent reformation of the transiently broken C_{11}═C_{12} π-bond that occurs in less than 500 fs and was thereby inaccessible to other structurally sensitive techniques.[1] Importantly, FSRS is a coherent spectroscopy in which changes in the vibrational frequencies that occur faster than the vibrational dephasing time can be detected because of the phase shifts and hence interference patterns that they produce in the resultant spectra. In rhodopsin, frequency sweeps occurring within the free induction decay (FID) of the probed vibration produce dispersive lineshapes via the heterodyned detection of the Raman signal with the probe pulse acting as a local oscillator.[13] The critical advance of the FSRS rhodopsin study was the observation of spectral shifts occurring in the hydrogen-out-of-plane (HOOP) vibrations near the point of isomerization. It was found that the C_{10}, C_{11}, and C_{12} HOOPs have an extremely weak restoring force 200 fs after excitation, shortly after the isomerization, and that the restoring force increases dramatically as the π-bond reforms and the carbon backbone relaxes on the 200−500 fs time scale. The frequency upshift of these modes was simulated and found to be consistent with an exponential frequency shift of these vibrations occurring with a 325 fs time constant.

In this work, we present a corrected functional form for the vibrational phase that is consistent with the physical picture of a time-dependent instantaneous frequency of the HOOP vibrations. We also show that the mathematical treatment of the phase of the HOOP vibrations was incorrect in ref 1. Using the corrected model, we recalculate the best vibrational parameters to fit the previously measured HOOP FSRS spectra.

THEORY

Previous simulations of the time-dependent frequency shifts observed using FSRS determined the vibrational phase, that is,

Received: March 25, 2011
Revised: June 7, 2011
Published: June 08, 2011

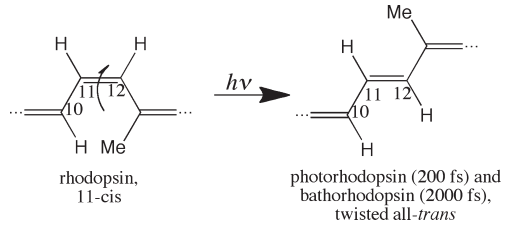

Figure 1. Primary event in vision. When the 11-*cis* retinal chromophore in rhodopsin absorbs a visible photon, it isomerizes to a twisted all-trans conformation, which initiates the visual response. Only the central portion of the extended retinal molecule is shown, to highlight the hydrogens whose vibrations produce strong hydrogen out-of-plane signals in the FSRS spectra.

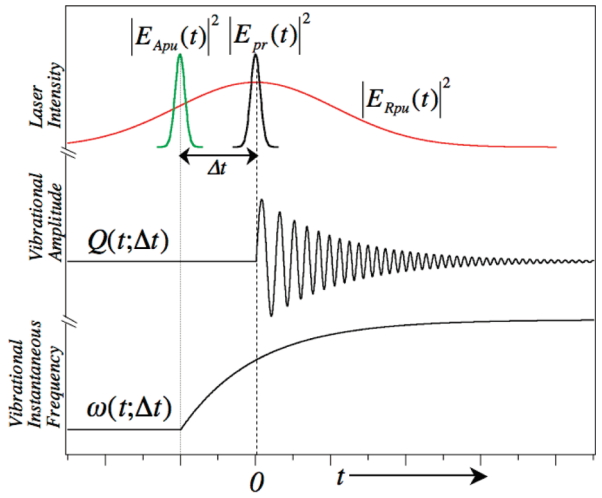

Figure 2. Schematic of theoretical treatment. The photochemistry is initiated by the actinic pump (green, top) that arrives at $t = -\Delta t$. Subsequently, the FSRS transition is initiated when the probe (black, top) arrives concurrent with the peak of the Raman pump pulse envelope (red, top) at the sample at $t = 0$. The molecular vibration displacement, $Q(t; \Delta t)$ (middle), is driven into coherence by the force of the Raman pump and probe and then dephases with an exponential decay. During the vibrational free-induction decay, the instantaneous frequency of the vibration shifts according to $\omega(t;\Delta t)$ (bottom). The changes in vibrational frequency within the free-induction decay induce phase changes that produce interference patterns in the detected FSRS spectral peak, which is detected in the optical frequency domain.

the argument of the cosine function, by multiplying the expected frequency shift by time. Hence, an oscillator with time-dependent frequency, $\omega(t)$, was assumed to have a vibrational phase of simply $\omega(t) \cdot t$. It was expected that the frequency of the HOOP modes would shift from the initial low-frequency, large-period value to the high-frequency, short-period values with first-order kinetics. A schematic of the theoretical treatment is shown in Figure 2. The period of the vibration was modeled with

$$\tau^{vib}(t) = \begin{cases} \tau_i, & t > -\Delta t \\ \tau_f + (\tau_i - \tau_f)e^{-(t+\Delta t)/\Gamma}, & t > -\Delta t \end{cases} \quad (1)$$

in which τ_i is the initial period; τ_f is the final period; and Γ is the time constant for relaxation between the two states. We have also adopted the convention of Kukura et al. in which the $t = 0$ is determined by the time that the probe arrives at the sample, so that the term $(t + \Delta t)$ is used to shift the beginning of the dynamics, effectively modeling the prior arrival of the pump pulse $t = -\Delta t$. (Note that there was a typo in the equation presented in the supporting online material of ref 1, in which the "$+\Delta t$" term was left out of the numerator of the exponent. In general, we will try to use the same notation as Kukura et al. to facilitate comparison.) In ref 1, the oscillations of the HOOP normal coordinate were modeled as

$$Q_{vib}(t) = \begin{cases} 0, & \text{for } t < 0 \\ exp\left(\frac{-t}{T_2}\right) \cdot cos\left(\frac{2\pi \cdot t}{\tau_{vib}(t)}\right), & \text{for } t > 0 \end{cases} \quad (2)$$

Using this model, the spectra were simulated, and τ_i, τ_f, Γ, and T_2 were adjusted to get the best fit to the observed spectra. In this model, the observed FSRS peak is generated from the FID of the vibration that initiates at $t = 0$ and decays exponentially with dephasing time constant T_2.

However, this model from ref 1 assumes that $\tau^{vib}(t)$ represented the "instantaneous" period of the evolving vibration, i.e., the inverse of the instantaneous frequency. Instead, the instantaneous frequency of a sinusoidal oscillation with a time-dependent frequency is

$$\omega(t) = \frac{d}{dt}\varphi(t) \quad (3)$$

which requires that the phase, ϕ, evolves according to

$$\varphi(t) = \int_0^t \omega(t)dt \quad (4)$$

In ref 1, it was assumed that the phase was simply

$$\varphi(t) = \omega(t) \cdot t = \frac{2\pi \cdot t}{\tau_{vib}(t)} = \frac{2\pi \cdot t}{\tau_f + (\tau_i - \tau_f)e^{-(t+\Delta t)/\Gamma}} \quad (5)$$

In which case the instantaneous frequency is actually

$$\omega(t) = \frac{d}{dt}\varphi(t) = \frac{d}{dt}\left[\frac{2\pi \cdot t}{\tau_f + (\tau_i - \tau_f)e^{-(t-\Delta t)/\Gamma}}\right] \quad (6)$$

or

$$\omega(t) = \frac{2\pi}{\tau_f + (\tau_i - \tau_f)e^{-(t+\Delta t)/\Gamma}} + \frac{2\pi(\tau_i - \tau_f) \cdot t \cdot e^{-(t+\Delta t)/\Gamma}}{\Gamma(\tau_f + (\tau_i - \tau_f)e^{-(t+\Delta t)/\Gamma})^2} \quad (7)$$

The first term in eq 7 is the intended time-dependent frequency, but the second term, which is always positive at $t > 0$ and $(\tau_i - \tau_f) > 0$, indicates that the actual instantaneous frequency of the model is higher than originally interpreted. Additionally, this instantaneous frequency is qualitatively not physically reasonable because at the same time delay relative to the actinic pump, $t + \Delta t$, the FID has a different instantaneous frequency depending on the pump−probe delay, Δt. For instance, the C_{10} HOOP has an instantaneous frequency of 816 cm^1 at $t = 100$ fs and $\Delta t = 200$ fs (that is 100 fs after the probe and 300 fs after the actinic pump) but 806 cm^{-1} at $t = 50$ fs, $\Delta t = 250$ fs (50 fs after the probe and 300 fs after the pump). In other words, the instantaneous frequency is different 100 fs into the FID in the experiment with a 200 fs pump−probe time delay than it is 50 fs into the FID in a 250 fs pump−probe time delay. This variation violates the foundational principle of the experiment: that the frequencies

dx.doi.org/10.1021/jp2028164 |J. Phys. Chem. B 2011, 115, 9299–9305

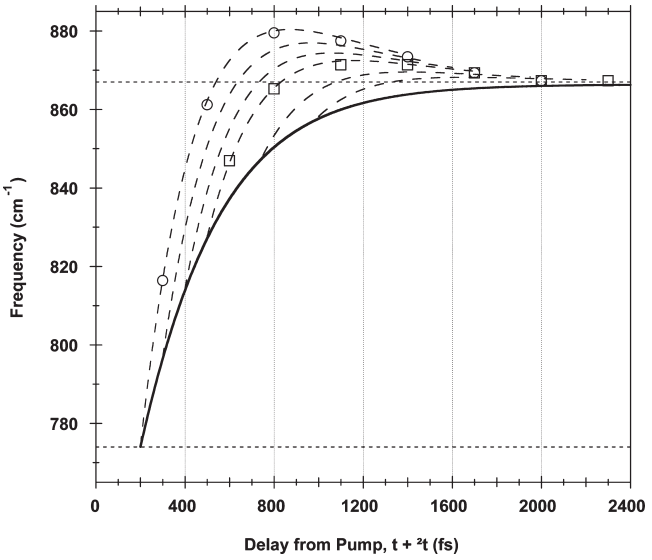

Figure 3. Time-dependent frequency of the $C_{10}H$ HOOP in the mathematical model of ref 1. The nominal 325 fs shift from 774 at 200 fs to the 867 cm^{-1} terminal frequency is shown as the dark solid line. The dashed curves show the actual instantaneous frequency calculated using eq 7, initiating at Δt = 200, 300, 400, 500, 750, and 1000 fs. Circles and squares indicate the instantaneous frequency evaluated by windowed Fourier transformation of eq 2 with Δt = 200 and 500 fs, respectively.

observed in the FID are the natural frequencies of the photoproduct at a particular time point in the reaction following the reaction's initiation by the actinic pump pulse.

These considerations are highlighted in Figure 3, which shows the intended frequency shift of the C_{10} HOOP, for which τ_i = 47 fs, τ_f = 38.5 fs ($\tilde{\nu}_i$ = 710 cm^{-1} and $\tilde{\nu}_f$ = 866 cm^{-1}), and Γ = 325 fs were determined in the original work. Also shown is the actual instantaneous frequency determined from eq 7. Clearly, the instantaneous frequency increases much more rapidly than the 325 fs time constant would imply. Also, the instantaneous frequency is seen to actually overshoot the final frequency between 450 and 2000 fs, an artifact of the model that is not physically reasonable. The overshoot is most significant for small Δt, reaching a maximum frequency of 880 cm^{-1} at $t + \Delta t$ = 800 fs when Δt = 200 fs (i.e., 600 fs into the FID of a Δt = 200 fs experiment). To corroborate the derivation of eq 6, we have computed the instantaneous frequency of eq 2, by directly computing eq 2 and then Fourier transforming the result using a Gaussian window function to select 100 fs regions at particular times (circles and squares, Figure 3). The numerical Fourier transforms confirm the calculus of eq 7.

To correct these problems with the previous simulations, it is only necessary to integrate eq 3, given an appropriate physical model of the frequency shift, $\omega(t)$. For rhodopsin, the intended physical model is essentially just that of eq 1: an exponential shift from one instantaneous frequency to another

$$\omega(t) = \begin{cases} \omega_i, & t < -\Delta t \\ \omega_i + \Delta\omega\left(1 - e^{-(t+\Delta t)/\Gamma}\right), & t > -\Delta t \end{cases} \quad (8)$$

where ω_i is the initial frequency at $t + \Delta t = 0$, and $\Delta\omega = \omega_f - \omega_i$. Hereafter, we only treat the experimentally probed times corresponding to the second line of eq 8, in which $t > -\Delta t$. The phase for the $\cos(\phi(t))$ term is

$$\begin{aligned} \varphi(t) &= \int_0^t \{\omega_i + \Delta\omega(1 - e^{-(t+\Delta t)/\Gamma})\}dt \\ &= \omega_i \cdot t + \Delta\omega \cdot t - \Gamma\Delta\omega(1 - e^{-(t+\Delta t)/\Gamma}) \end{aligned} \quad (9)$$

Here we have changed from modeling the time-dependent period, as in eq 1, to the time-dependent frequency, which allows simpler notation. Equation 9 now fits a physically intuitive model, in that the instantaneous frequency is constant for a given time delay from excitation, $t + \Delta t$, independent of the partitioning of that delay into the pump−probe delay, Δt, and the FID time, t.

The FSRS line shape is generated using established spectroscopic theory.[1,13] The signal electric field, E_{FSRS}, is generated by the oscillatory vibrational amplitude that modulates the molecular polarizability according to

$$\begin{aligned} E_{FSRS}(t) &= b \cdot E_{RPu}(t) \cdot \sum_i \alpha_i' \cdot Q_i(t) \\ &= b \cdot E_{RPu}(t) \cdot \sum_i \alpha_i' \, exp\left(\frac{-t}{T_{2,i}}\right) \cdot cos(\omega_i \cdot t + \Delta\omega_i \cdot t \\ &\quad - \Gamma_i\Delta\omega_i(1 - e^{-(t+\Delta t)/\Gamma_i})) \end{aligned} \quad (10)$$

in which b subsumes several constants from the wave equation; E_{RPu} is the electric field of the Raman pump pulse; α_i' is the derived molecular Raman polarizability of mode i, $d\alpha/dQ_i$; and $Q_i(t)$ is the vibrational amplitude of mode i. In the second line, we have expanded the expression for $Q_i(t)$ to include the phase $\phi(t)$ from eq 9 and exponential damping with time constant T_2. The measured *spectrum* is the intensity of the sum of the FSRS signal and probe fields normalized by the probe field intensity

$$\Delta I_{FSRS}(\omega) = \frac{|E_{FSRS}(\omega) + E_{pr}(\omega)|^2}{|E_{pr}(\omega)|^2} \quad (11)$$

Here, we have Fourier transformed the time-dependent signal and laser fields, $E_x(t)$, to the frequency domain, $E_x(\omega)$. The spectra presented below are calculated using eqs 10 and 11, incorporating Gaussian laser pulses with the Raman pump centered at 800 nm and having a 3 ps intensity full-width at half-maximum (fwhm) and the probe centered at 900 nm and having a 20 fs fwhm. The resulting spectrum is arbitrarily scaled to match the observed signal intensities, so that the lineshapes can be compared.

RESULTS AND DISCUSSION

The important difference from the previously reported results is the estimated rate of change of the instantaneous frequency. Kukura et al. report a 325 fs time constant for the frequency shift of the HOOP modes as rhodopsin relaxes from photo to batho. In fact, as seen in Figure 3, the instantaneous frequencies of their model shift much more quickly than the 325 fs time constant would imply. We can estimate an actual time constant for the shift to be 150−160 fs, obtained by fitting the instantaneous frequency curves for $t > 0$ (Figure 3) to a single exponential rise. This value is refined to ~140 fs by fitting the complete HOOP spectral region (vide infra).

Figure 4 compares the lineshapes of the C_{10} hydrogen-out-of-plane (HOOP) vibration generated using the old (eq 5) and new (eq 9) phases. At Δt = 200 fs, the old line shape (dashed line) produces a negative feature at 879 cm^{-1}, due to the overshoot in

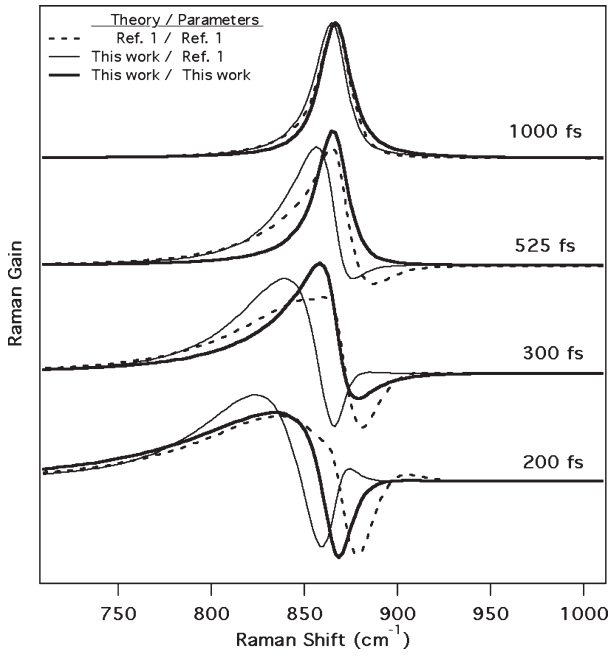

Figure 4. Simulated line shape of the C_{10} hydrogen-out-of-plane (HOOP) mode using the old and new models, from refs 1 and eq 9, respectively. Dashed line: theory and parameters from ref 1: $\nu(200\text{ fs}) = 772\text{ cm}^{-1}$, $\nu(\infty) = 867\text{ cm}^{-1}$, $\Gamma = 325$ fs, $T_2 = 620$ fs. Thin solid lines are calculated using the corrected theory (eq 9) and the parameters from ref 1. Thick solid lines are calculated using the corrected theory (eq 9) and the best parameters determined in this work: $\nu(200\text{ fs}) = 757\text{ cm}^{-1}$, $\nu(\infty) = 870\text{ cm}^{-1}$, $\Gamma = 140$ fs, $T_2 = 620$ fs.

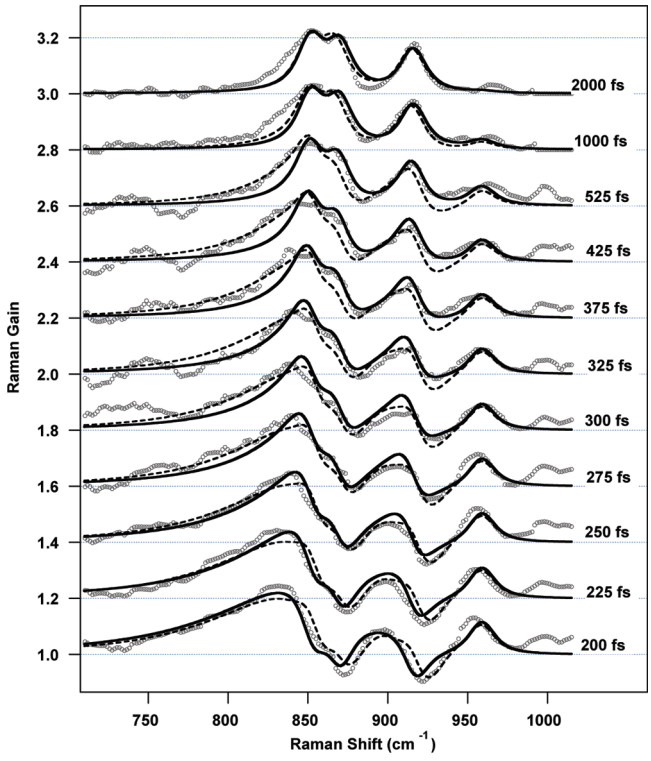

Figure 5. Simulated FSRS spectra of the photorhodopsin to bathorhodopsin transition for $\Delta t = 200-2000$ fs. Dashed lines are simulations using the original phase expression from ref 1 (eqs 1 and 2) and the original parameters; solid lines are the revised theoretical treatment and the revised parameters (eq 9 and Table 1). Gray circles are the experimental data. Each spectrum is offset vertically by 0.2 for clarity.

the instantaneous frequency shown in Figure 3. In contrast, when the corrected phase is used with the exact same parameters (thin solid line, Figure 4), this negative feature occurs at 859 cm^{-1}, i.e., below the terminal frequency of 867 cm^{-1}. This behavior is expected since the physical model implies a monotonic increase in the frequency from 774 cm^{-1} at 200 fs to 867 cm^{-1} at long times with time constant, Γ, of 325 fs. However, the thin solid lines in Figure 4 show that using Kukura et al.'s parameters in the new model produces a line shape at 200 and 300 fs that has too much intensity and is too sharply peaked on the low frequency shoulder of the peak. Additionally, at 200 fs the 325-fs time constant for the shift produces a positive peak at 875 cm^{-1} that is not seen in the data. Instead, if we accomplish nearly the same magnitude of spectral shift with a $\Gamma = 140$ fs time constant (thick solid lines, Figure 4), the line shape reproduces the broad low-frequency shoulder in the 200 fs spectrum and the negative dip shifts to higher frequency. The 140 fs time constant is the optimized value of Γ determined by reproducing the full spectrum of the C_{10}, C_{11}, and C_{12} HOOP region (see below).

To evaluate the implications of this new vibrational phase, the parameters of the C_{10}, C_{11}, and C_{12} HOOP region were adjusted to give the best fit to the experimental data (Figure 5). Because of the highly nonlinear nature of the line-shape and its nonlinear dependence on the FID parameters, it was not possible to determine the best global fit in an automated least-squares method. Instead, as in the original work, each parameter was adjusted until the gross features of the spectra were fit as well as possible. The final values of the line shape parameters are shown in Table 1. Several changes are visible in comparing the new parameters to the original results. Most significant is the time constant for the spectral shift, Γ, which was determined to be 325 fs in the original work but we determine to be

Table 1. Simulation Parameters Determined from Fitting the Spectra[a]

simulation parameter	ref 1	this work
time constant for spectral upshift, Γ (fs)	325	140 ± 20
vib. dephasing time, T_2 (fs)	620	620
C_{10}—HOOP frequency at 200 fs (cm^{-1})	772	757 ± 20
C_{10}—HOOP frequency at 2000 fs (cm^{-1})	867	870 ± 3
C_{11}—HOOP frequency at 200 fs (cm^{-1})	811	812 ± 20
C_{11}—HOOP frequency at 2000 fs (cm^{-1})	915	916 ± 3
C_{12}—HOOP frequency at 200 fs (cm^{-1})	762	751 ± 20
C_{12}—HOOP frequency at 2000 fs (cm^{-1})	851	852 ± 3

[a] Additional parameters remained nearly the same in the new fits: Hot rho 11 = 12 HOOP frequency = 590 cm^{-1}, intensity = 0.0053, decay time, T_2 = 600 fs; Intensity of C_{10}—HOOP = 0.0042, C_{11}—HOOP = 0.0045, C_{12}—HOOP = 0.0044; Raman pump pulse = 800 nm, 3000 fs; Probe pulse = 900 nm, 20 fs.

140 ± 20 fs. Additionally, the C_{10}—HOOP and C_{11}—HOOP modes are best modeled with initial frequencies at 200 fs that are 10—15 cm^{-1} below the values originally determined. However, because of the insensitivity of the spectra to these initial frequencies, their precision is estimated as only $\pm 20\text{ cm}^{-1}$, and the frequency difference from the original work is insignificant. All other parameters are approximately the same as they were in the original work.

Examining the spectra in Figure 5, we can see both improvements and degradation in the quality of the new fit to the data.

dx.doi.org/10.1021/jp2028164 |J. Phys. Chem. B 2011, 115, 9299–9305

The original simulations consistently produce a large negative feature at 930 cm^{-1} that is inconsistent with the observed spectra from 300 to 525 fs. This feature is more easily seen in Figure 4, in which the old simulation parameters consistently produce a negative feature on the high-frequency side of the peak, even at a time delay of 525 fs. Our new simulations do a better job of fitting the spectra in this region while at the same time fitting the broad low-frequency shoulder from 750 to 830 cm^{-1} seen at delays from 200 to 250 fs. The main failing of the new model is its inability to fit the full width of the 850 cm^{-1} band at delays of 300−1000 fs. However, it is expected that at these time delays a great deal of thermal inhomogeneity would be implicit in the spectra.[14] The spectral simulations here and in the original work do not include this effect, and so the disparity in the fit is expected. In the original work, the ability of the simulation to produce this broad shoulder is simply a fortuitous coincidence of an artifact in the model. As shown in Figure 3, the original simulations produce FIDs with consistently fast exponential rise times that overshoot the terminal frequency. This artifact produces spectra that have large low-frequency shoulders even at long time delays when there should be only small spectral shifts during the FID.

Because our new simulations reproduce the broad low-frequency shoulder at short times and the high-frequency negative dip at all times, we consider them to be improved relative to the previous parameters. However, an ideal simulation would need to include both (1) the effect of thermal inhomogeneity from 300 to 1000 fs and (2) the anharmonic coupling expected between the HOOP modes and the coherently oscillating 60 cm^{-1} torsional mode, which is known to oscillate coherently for 1−2 ps after photoexcitation.[4] The thermal inhomogeneity is expected to produce a down-shift and broadening of spectral features as the system equilibrates the excess photon energy deposited in the molecular network. Such inhomogeneity is unaccounted for in these simulations and would require knowledge of the time-dependent dephasing time as well as the spectral inhomogeneity. As has been theoretically predicted for 2D-FSRS experiments, anharmonic coupling between the vibrationally coherent torsion and the observed HOOPS or coherent Raman cascades could produce sidebands up- and down-shifted by ±60 cm^{-1} from each HOOP vibration.[15,16] In this case, each sideband could have a time-dependent positive, negative, or dispersive line shape that depended on the relative phase of the coherent torsion and the HOOP modes. However, it is very unlikely that any such sidebands are present in the rhodopsin FSRS spectra because none of the unaccounted-for wiggles in the spectral baseline occur where one would expect sidebands, i.e., at 870 ± 60, 916 ± 60, or 852 ± 60 cm^{-1}, and the fundamental transitions have relatively small intensity compared to those probed in 2D-FSRS.

Our revised time constant of 140 fs for the spectral shift occurring in the photoproduct spectra implies that the equilibrium structure of the bathorhodopsin chromophore is reached more quickly than previously thought. In other words, after the photoproduct first appears (∼150−200 fs after the absorption of the initial actinic photon) the ballistic, or coherent, portion of the isomerization is complete in roughly 140 fs. Time-resolved spontaneous anti-Stokes Raman studies have shown that the photoproduct HOOP vibrations are excited both directly by the isomerization and later via vibrational relaxation of higher frequency modes in 1.2 ps.[14] The resultant HOOP vibrational excitation then dissipates in ∼2.7 ps.[14] This indicates that the 140 fs spectral shift observed in the FSRS HOOP spectra cannot simply be assigned to coherent vibrational relaxation within the HOOP vibrational manifold. If this were the case, then no anti-Stokes intensity would be present after 140 fs. Instead, after 140 fs, an incoherent but vibrationally excited HOOP population must be established, whose vibrational relaxation proceeds via normal incoherent molecular pathways. We must also reconcile the FSRS data with the observation of long-lived low-frequency coherence in a ∼60 cm^{-1} skeletal torsion that modulates the transient absorption signal with a 550 fs period[4,9,10,17] and the simultaneous lack of modulation of the FSRS spectrum with this same period. This indicates that the HOOP vibrational dephasing time, 620 fs, is long enough that any modest frequency modulation is averaged out in the observed spectrum. Finally, it is striking that there is a consistent ∼100 cm^{-1} shift in each of the three observed HOOP vibrations, despite the calculations of Yan et al. that indicated that the ∼852 cm^{-1} C_{12}−HOOP frequency is dramatically shifted depending on the C_{10}═C_{11}−C_{12} backbone twist.[7] Those calculations found that the frequency of the C_{11}−HOOP at 915 cm^{-1} was very insensitive to the backbone twist, implying that it should arrive at its final frequency while the C_{12}− and C_{10}−HOOPs are still up-shifting to their final values. Despite this inconsistency, the dramatic time-dependent shifts implicit in the FSRS spectra indicate that after the chromophore drops into the photoproduct potential well it spends approximately 140 fs migrating monotonically toward the equilibrium backbone geometry of bathorhodopsin. Once there, it oscillates around the equilibrium for 1−2 ps as it dissipates the excess vibrational energy deposited by the rapid internal conversion process.

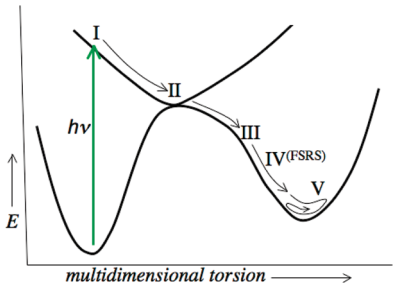

Figure 6. Schematic diagram of the reaction coordinate of rhodopsin. The Franck−Condon state (I) is reached upon absorption of a photon. The conical intersection with the ground state (II) is reached 80−110 fs after photon absorption, but the first appearance of the characteristic photoproduct absorption spectrum (III) does not occur until 150−200 fs after photon absorption. After its initial appearance, the photoproduct approaches its equilibrium backbone structure with a 140 fs time constant ($IV^{(FSRS)}$) that is probed in the FSRS experiments. Finally, after reaching the equilibrium backbone structure, the chromophore coherently oscillates around that equilibrium for ∼2000 fs.

The overall reaction kinetics of rhodopsin are summarized in Figure 6. Transient absorption and quantum dynamics simulations have indicated that after the system absorbs light, placing it on the excited state Franck−Condon surface at Δt = 0 fs (I, Figure 6), it relaxes to a conical intersection with the ground state in 80−110 fs (II).[10,18] After dropping to the ground-state surface, there is a broad red-shifted absorption band that eventually coalesces to produce the first identifiable photoproduct absorption band by Δt = 150−200 fs (III). At this point, the FSRS experiment found a dramatic upshift in the HOOP frequencies that occurs with a 140 fs time constant between Δt = 200 and 500 fs ($IV^{(FSRS)}$).[1] It is on this time-scale that the backbone π-conjugation recovers so that the HOOP restoring force increases. Finally, between 500 and 2000 fs (V), the photoproduct oscillates coherently around the photoproduct equilibrium

structure as intramolecular vibrational energy redistribution and cooling dissipate the excess energy from the system.[4,10,14]

The time it takes to reach the equilibrium backbone geometry in bathorhodopsin is a directly testable hypothesis that should be investigated further in computational quantum simulations. Experimentally, it has been shown that the conical intersection is reached at around 80 fs but that the characteristic absorption spectrum of all-trans photoproduct does not appear until 200 fs.[10] Additionally, these FSRS simulations indicate that after its appearance at 200 fs the photoproduct continues to structurally evolve, only reaching its equilibrium structure at times longer than $\Delta t \sim 340$ fs (i.e., 140 fs following the appearance of the photoproduct). The dynamics of approaching and departing from the conical intersection have been a significant focus of many high-level quantum dynamics simulations.[10,18−28] These simulations indicate that the equilibrium backbone structure is reached very rapidly, within 50−80 fs, following the S_1-S_0 decay at the conical intersection. Our new estimation of a 140 fs time constant for this relaxation is much closer to these computational results than the previous 325 fs value in ref 1. However, quantum dynamics studies generally do not discuss this aspect of the isomerization, focusing instead on the time it takes to reach the conical intersection, the shape of the excited state potential energy surface, and the role that atomic momentum plays in the photochemical outcome. Additionally, because of the expense of the simulations, most trajectories end at ∼200 fs, which is insufficient to appropriately model the photoproduct equilibration. Our reassessment of the rapidity of the equilibration will hopefully spur further dynamics simulations to present directly comparable quantities, such as HOOP instantaneous frequencies, at time delays up to 500 fs as the photoproduct relaxes in the ground-state potential energy surface.

Finally, we should address the inherent time resolution in FSRS since, while this manuscript was under review, a communication by Mukamel and Biggs was published that discusses this important issue.[29] In previous work by McCamant, Kukura, Lee, Mathies, and co-workers, it has been shown that the FSRS lineshape is produced over the entire dephasing time, T_2, of the probed vibration, perhaps truncated by the Raman pump pulse duration.[1,12,13,30] Ignoring potential broadening from the resolution of the spectrograph and detection system, this implies that the FSRS spectral resolution is a convolution of the inherent molecular line shape, including T_2 broadening *and* inhomogeneity, and the spectral bandwidth of the Raman pump. As in any time-resolved spectroscopy in which the laser pulses are much shorter than the relevant dephasing times, the "time resolution" of the experiment is not simply the time over which the signal is generated, which is typically 0.5−3 ps for vibrational spectroscopies like FSRS. Instead, in any such technique, one can only precisely control the time at which the coherences are initiated, after which each coherence will evolve with its own inherent dephasing time. As with femtosecond time-resolved infrared spectroscopy (TRIR), "time resolution" in FSRS refers to the precision with which one can control the delay between when a photochemical event is started and when the vibrational transition is *initiated*. As such, it is measured by the convolution of the actinic-pump pulse envelope and that of the probe pulse. Certainly, as Mukamel and Biggs point out, it is wrong to imply that the FSRS signal represents the instantaneous frequencies present in the sample only at the moment the probe arrives. As they point out, and is reiterated herein and in previous work by Mathies and co-workers, the observed FSRS line shape is representative of the vibrational frequencies present in the sample over the course of the vibrational dephasing time, T_2, gated by the Raman-pump pulse. The ability of FSRS to extract vibrational frequency shifts that occur faster than the vibrational dephasing time is due entirely to the heterodyned detection system, in which the Raman signals are detected on top of the original probe field that initiated the Raman coherence. This heterodyned detection allows interference and thereby negative FSRS signals, which can be deconvoluted to reveal the time-dependent molecular frequencies. Importantly, these same interference signals should be visible in TRIR work, in which a pump−probe beam geometry is used and the IR signal is dispersed on a multichannel detector after the sample. This is because absorption is also a self-heterodyned technique in which a vibrational coherence is induced by the action of a short broadband IR pulse, and the subsequent narrow bandwidth IR radiation emitted by the sample is detected on top of the spectrum of the IR pulse that drove the coherence in the first place. Yet, to our knowledge no such dispersive lineshapes have been observed in TRIR to date.

CONCLUSION

We have shown that a corrected mathematical treatment of the theory of FSRS is necessary for situations in which there is a significant frequency change during the Raman vibrational free induction decay. With this new theory, the time-dependent FSRS lineshapes of rhodopsin can be simulated, revealing that each HOOP mode relaxes on the photoproduct potential energy surface with a 140 fs time constant, during which each mode experiences a $\sim 100\ cm^{-1}$ upshift in its instantaneous frequency. These simulations imply that the equilibrium structure of the rhodopsin photoproduct, a twisted all-*trans* retinal chromophore, is reached ∼140 fs after the initial photoproduct absorption spectrum appears. This time constant represents an important experimental constraint that should be examined by further quantum dynamics simulations.

AUTHOR INFORMATION

Corresponding Author

*E-mail: mccamant@chem.rochester.edu.

ACKNOWLEDGMENT

The author gratefully acknowledges financial support from the Alfred P. Sloan Foundation, the National Institutes of Health (5R21RR025344), the National Science Foundation (CHE-0845183), and the University of Rochester, as well as helpful discussions with Philipp Kukura and Richard A. Mathies.

REFERENCES

(1) Kukura, P.; McCamant, D. W.; Yoon, S.; Wandschneider, D. B.; Mathies, R. A. *Science* **2005**, *310*, 1006–1009.

(2) Kandori, H.; Shichida, Y.; Yoshizawa, T. *Biochemistry (Moscow)* **2001**, *66*, 1197–1209.

(3) Peteanu, L. A.; Schoenlein, R. W.; Wang, Q.; Mathies, R. A.; Shank, C. V. *Proc. Natl. Acad. Sci. U.S.A.* **1993**, *90*, 11762–11766.

(4) Wang, Q.; Schoenlein, R. W.; Peteanu, L. A.; Mathies, R. A.; Shank, C. V. *Science* **1994**, *266*, 422–424.

(5) Kim, J. E.; McCamant, D. W.; Zhu, L.; Mathies, R. A. *J. Phys. Chem. B* **2001**, *105*, 1240–1249.

(6) Eyring, G.; Curry, B.; Broek, A.; Lugtenburg, J.; Mathies, R. *Biochemistry* **1982**, *21*, 384–393.
(7) Yan, E. C. Y.; Ganim, Z.; Kazmi, M. A.; Chang, B. S. W.; Sakmar, T. P.; Mathies, R. A. *Biochemistry* **2004**, *43*, 10867–10876.
(8) Kandori, H.; Furutani, Y.; Nishimura, S.; Shichida, Y.; Chosrowjan, H.; Shibata, Y.; Mataga, N. *Chem. Phys. Lett.* **2001**, *334*, 271–276.
(9) Haran, G.; Morlino, E. A.; Matthes, J.; Callender, R. H.; Hochstrasser, R. M. *J. Phys. Chem. A* **1999**, *103*, 2202–2207.
(10) Polli, D.; Altoe, P.; Weingart, O.; Spillane, K. M.; Manzoni, C.; Brida, D.; Tomasello, G.; Orlandi, G.; Kukura, P.; Mathies, R. A.; et al. *Nature* **2010**, *467*, 440–443.
(11) Kukura, P.; McCamant, D. W.; Mathies, R. A. *Annu. Rev. Phys. Chem.* **2007**, *58*, 461–488.
(12) McCamant, D. W.; Kukura, P.; Yoon, S.; Mathies, R. A. *Rev. Sci. Instrum.* **2004**, *75*, 4971–4980.
(13) Lee, S. Y.; Zhang, D.; McCamant, D. W.; Kukura, P.; Mathies, R. A. *J. Chem. Phys.* **2004**, *121*, 3632–3642.
(14) Kim, J. E.; Mathies, R. A. *J. Phys. Chem. A* **2002**, *106*, 8508–8515.
(15) Wilson, K.; Lyons, B.; Mehlenbacher, R.; Sabatini, R.; McCamant, D. M. *J. Chem. Phys.* **2009**, *131*, 214502.
(16) Mehlenbacher, R.; Lyons, B.; Wilson, K.; Yong, D.; McCamant, D. M. *J. Chem. Phys.* **2009**, *131*, 244512.
(17) Wang, Q.; Schoenlein, R. W.; Peteanu, L. A.; Mathies, R. A.; Shank, C. V. *Biophys. J.* **1993**, *64*, A127–A127.
(18) Weingart, O.; Schapiro, I.; Buss, V. *J. Phys. Chem. B* **2007**, *111*, 3782–3788.
(19) Tomasello, G.; Olaso-Gonzalez, G.; Altoe, P.; Stenta, M.; Serrano-Andres, L.; Merchan, M.; Orlandi, G.; Bottoni, A.; Garavelli, M. *J. Am. Chem. Soc.* **2009**, *131*, 5172–5186.
(20) Garavelli, M.; Vreven, T.; Celani, P.; Bernardi, F.; Robb, M. A.; Olivucci, M. *J. Am. Chem. Soc.* **1998**, *120*, 1285–1288.
(21) Garavelli, M.; Celani, P.; Bernardi, F.; Robb, M. A.; Olivucci, M. *J. Am. Chem. Soc.* **1997**, *119*, 6891–6901.
(22) Hahn, S.; Stock, G. *J. Phys. Chem. B* **2000**, *104*, 1146–1149.
(23) Chen, X.; Batista, V. S. *J. Photochem. Photobiol. A* **2007**, *190*, 274–282.
(24) Virshup, A. M.; Punwong, C.; Pogorelov, T. V.; Lindquist, B. A.; Ko, C.; Martinez, T. J. *J. Phys. Chem. B* **2009**, *113*, 3280–3291.
(25) Weingart, O.; Buss, V.; Robb, M. A. *Phase Transitions* **2005**, *78*, 17–24.
(26) Weingart, O.; Schapiro, I.; Buss, V. *J. Mol. Model.* **2006**, *12*, 713–721.
(27) Hayashi, S.; Taikhorshid, E.; Schulten, K. *Biophys. J.* **2009**, *96*, 403–416.
(28) Frutos, L. M.; Andruniow, T.; Santoro, F.; Ferre, N.; Olivucci, M. *Proc. Natl. Acad. Sci. U.S.A.* **2007**, *104*, 7764–7769.
(29) Mukamel, S.; Biggs, J. D. *J. Chem. Phys.* **2011**, *134*, 161101–4.
(30) Yoon, S.; McCamant, D. W.; Kukura, P.; Mathies, R. A.; Zhang, D.; Lee, S. Y. *J. Chem. Phys.* **2005**, *122*, 24505.